ARCHIVES OF TRANSPORT *ISSN (print):* *0866-9546*
Volume 63, Issue 3, 2022 ***e-ISSN (online):*** *2300-8830*
DOI: *10.5604/01.3001.0016.0019*

FUEL SAVING INDEX ASSESSMENT ON DRIVING BEHAVIOR CONTROL SYSTEM OF PROTOTYPE MODEL USING NEURAL NETWORK

Suroto MUNAHAR [1], Aris TRIWIYATNO[2], M. MUNADI[3], Joga Dharma SETIAWAN[4]

[1, 3, 4] *Department of Mechanical Engineering, Diponegoro University, Semarang, Indonesia*

[1] *Department of Automotive Engineering, Universitas Muhammadiyah Magelang, Magelang, Indonesia*

[2] *Department of Electronics Engineering, Diponegoro University, Semarang, Indonesia*

***Abstract**:*

Efficient fuel consumption in the world is essential in automotive technology development due to the increase in vehicle usage and the decrease in global oil production. Several studies have been conducted to increase fuel consumption savings, Fuel Cells (FCs), the application of alternative energy vehicles and the Engine Control Unit (ECU) system. FCs do not require oil energy to propel the vehicle, so this technology promises to reduce energy consumption and emissions. However, this research still leaves problems. FCs are susceptible to short circuit hazards, and ownership costs are very high. Alternative energy applications produce less power, less responsive acceleration, and insufficient energy sources to enter mass production. The ECU application still has an orientation toward achieving stoichiometry values, so the increase in fuel efficiency has the potential to be improved. Driving behavior is a variable that has a close relationship with fuel consumption efficiency. However, research on driving behavior is only studied for implementation in autonomous car-following technologies, safety systems, charging needs characteristic of electric vehicles, emission controls, and display images on in-vehicle information systems. Meanwhile, research on driving behavior as a control system to improve fuel efficiency has not been carried out. To that end, this study proposes the use of driving behavior for a newly designed control system to improve fuel efficiency. The control system in this research is a prototype model to be assessed using the Fuel Saving Index (FSI) analysis. An artificial neural network is used to help the recognition of driving behavior. The results showed that the newly designed control system was categorized on scale IV of FSI. On this scale, the power generated by the engine is quite optimal when it is in the eco-scheme driving behavior. The driving behavior control system can significantly improve the efficiency of fuel consumption. Air to Fuel Ratio (AFR) is achieved above the stoichiometric value.

Keywords: *Fuel Saving Index, FSI, Air to Fuel Ratio, AFR, stoichiometry, driving behavior, neural network*

To cite this article:

Munahar, S., Triwiyatno, A., Munadi, M., Setiawan, J.D. (2022). Fuel saving index assessment on driving behavior control system of prototype model using neural network. Archives of Transport, 63(3), 123-141. DOI: https://doi.org/10.5604/01.3001.0016.0019

Contact:
1) munahar@unimma.ac.id [https://orcid.org/0000-0002-8236-0741] – corresponding author; 2) aristriwiyatno@live.undip.ac.id [https://orcid.org/0000-0001-8666-2678]; 3) munadi@ft.undip.ac.id [https://orcid.org/0000-0002-0766-0955];
4) joga.setiawan@ft.undip.ac.id [https://orcid.org/0000-0002-2948-9204]

1. Introduction

The issue of fuel efficiency is presently a hot topic at the global level, especially in the development of automotive technology, where this energy performance is necessary (Uslu & Celik, 2020). The limited number and reduction of energy production also trigger the necessity of implementing efficiency (Alfattah, 2020). Although the need for vehicles continuously increases with the elevation of population growth. Many efforts have reportedly been conducted to solve this problem, including the development of FCs (Xiong et al., 2019; Sun et al., 2019). These are part of the exciting developments of science and technology breakthroughs, which have the potential to achieve good efficiency and emissions. The FCs do not have clear rules for mass production, as infrastructure and high prices are still the main obstacles. To improve this vehicular efficiency, another breakthrough involves the development of alternative power, including methanol and ethanol (Biswal et al., 2020). This research uses renewable energy and is processed from vegetable energy. From an economic point of view, the selling price and availability of energy are still not feasible to enter the market because it requires a long input time for mass production.

The development of other alternative energy also involves the application of gas fuels, such as LNG (Liquid Natural Gas), CNG (Compressed Natural Gas), and LPG (Liquid Petroleum Gas) (Mehra et al., 2018). LPG is a gaseous fuel that produces cleaner emissions and better efficiency. This study found that LPG produces cleaner emissions and better efficiency, although it has less power and acceleration than gasoline engine vehicles (Alper & Do, 2018; Nguyen & Nguyen, 2018).

Another study also involves the development of the ECU to control the fuel system (Robertson & Prucka, 2020). According to Dennis and Robert (Robertson & Prucka, 2020), AFR has a high potential in controlling efficiency. The ECU focused on the input of CPU-based sensors to regulate fuel performance. As the brain of fuel efficiency control, the Central Processing Unit (CPU) has reportedly been developed with several variables, including artificial intelligence (Sardarmehni et al., 2020); (Y. Wang et al., 2020), road conditions (Munahar et al., 2020), lambda achievement (λ) and vehicle dynamics (Ahmed & Al, 2019). Based on research (Y. Wang et al., 2020) and (Sardarmehni et al., 2019), efficiency was predicted using fuzzy to control AFR, although lean fuel mixtures were not considered. Despite this limitation, both studies still had the potential to improve efficiency. Meanwhile, improving the efficiency system based on road conditions can be achieved well. However, this research has not yet developed a driver behavior control program (Munahar et al., 2020). According to Ahmed (Ahmed & Al, 2019), the lambda value was oriented with 1, a comparison of the stoichiometry AFR. This study had good results, although the use of lean mixtures to improve fuel efficiency had not been assessed. Muji (Setiyo M. & Munahar, 2017) also developed a control system based on vehicle dynamics when operating on the highway, although the driver behavior aspect was not considered.

Furthermore, another improvement method was developed based on the predictions of driver behavior, which were assessed under various conditions (Xing et al., 2020). While (Xing et al., 2020) such as a close relationship between acceleration or deceleration with energy consumption. The results were still predictive, although not inputted into the system design direction. Meanwhile, another observation was provided on the driver behavior when a vehicular operation was carried out with several variables, including vehicle technology development of car following, safety systems, charging needs characteristic of electric vehicle, electric car drive system, as well as emission control, and display images on in-vehicle information systems.

Car following researcher (Zhao et al., 2020) observed the driving behavior when following another vehicle. The observed vehicles are autonomous vehicles and vehicles with human drivers. The results of the study concluded that subjective trust greatly influences driving behavior. However, fuel consumption has not been discussed in this study. (Sharma et al., 2019) and (Fadhloun & Rakha, 2020), a behavior control system was also developed for driving patterns when the driver decides to follow another vehicle. This research provides safe driving recommendations, although the factor of fuel use was not considered.

Next, researchers (Grove et al., 2019) and (Wang et al., 2020) also observed driver behavior when asleep, and the obtained results were subsequently used to develop a safety control feedback system. Furthermore, (Hong, Chen, & Wu, 2020) assessed

the safety behaviors needed to avert accidents, with (Martinelli et al., 2020) storing drivers' attitudes in a device after recording. The results indicated that the machine was immediately shut down when other behaviors were not identified due to the security system assuming that the vehicle had been stolen. According to (Yuan, Lu, & Wang, 2020), an adaptive Forward Vehicle Collision Warning (FCW) was developed to signal the driver when the behavior was dangerous. These five studies focused on identifying driver behaviors, although energy consumption was still not evaluated.

Based on (Ashkrof et al., 2020), the driver behavior was subsequently analyzed when selecting a road route to determine the charging system for EVs vehicles. This driver behavior character is useful for determining the planning location for the most effective EV filling station construction. This study focused on controlling the needs characteristics of electric vehicles on vehicular, although fuel efficiency was not carried out. Other researchers (Stogios et al., 2019) and (Monika et al., 2022) examined driver behavior towards changes in the generation of emissions. Subsequently, the study by (Kohl et al., 2020) analyzed display images on in-vehicle information systems on vehicle of driver behavior. These three studies looked at changes in driver behavior based on changes in emissions in traffic lights and graphical displays. However, development was not observed in the fuel consumption influenced by the behavior.

To improve fuel efficiency, several previous studies involved the development of EVs, FCs, as well as vehicular alternative energy, and ECU system applications. The improvement of driver behavior identification was consequently used to develop cars following technology, safety systems, vehicle control, emission control, and graphical displays. Several studies that have been conducted have not discussed fuel-efficiency control that considers driver behavior. This research needs to be done because the driver's behavior closely relates to fuel use, as stated by previous researchers (Xing et al., 2020). Therefore, this study proposes a new method by developing a prototype model of a driving behavior control system using a neural network based on FSI assessment. The neural network is embedded in the control system designed to recognize driving behavior. This study carries out the suggestions presented by Yang et al. (Xing et al., 2020) with the concepts shown in Fig. 1.

2. Methods

This study was designed in several stages: installing sensors, designing and installing a vehicular acceleration control system with the National Instruments (NI) MyRio microcontroller, obtaining actual signal data on driving behavior using data acquisition, designing vehicle engine modeling, and conducting training and embedded neural network in Integrated Circuit (IC) ATmega 328.

.

2.1. Equipment Calibration

The utilized equipment had several components for the control system, including sensors a microcontroller, and IC ATmega 328. The specifications of this equipment are shown in Table 1.

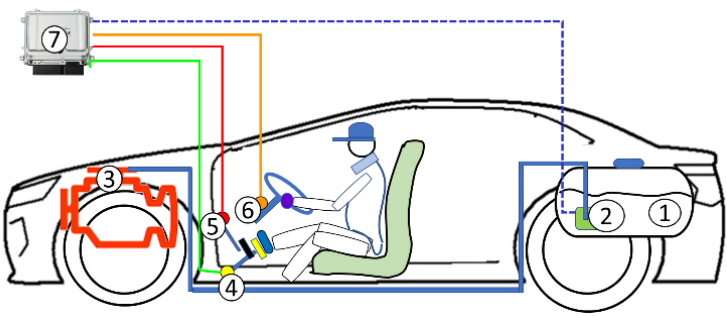

Description:
1. Fuel tank.
2. Fuel pumps.
3. Machine.
4. Throttle valve opening speed sensor.
5. Braking speed sensor.
6. Steering speed sensor.
7. Developed control system using neural network.

Fig. 1. The prototype concept of a driving behavior control system using a neural network

Table 1. The equipment specifications

No.	Information	Description	Specification
1.	Vehicle type	Engine type	Gasoline
2.		Engine volume	1500 cc
3.		Vehicle type	Saloon car
4.		Number of cylinders	4 cylinders
5.		Engine cycle	4 stroke engines
6.	Speed sensor	Voltage	12 Volt
7.		Type	Gearbox
8.		Rotation	250 Rpm
9.		Output	5 Volt
10.		Dimension	137 x 86 x25 mm
11.	Microcontroller for driving	Processor	667 Mhz
12.	behavior recognition	Power Input	6 – 16 VDC/14 watt
13.		Analog input, resolution	500ks/s, 12 bits
14.		Product Type	NI MyRio 2015
15.		Memory DD3	533 MHz
16.	IC ATmega 328	RAM	2K Byte
17.		Power input	5 volt
18.		Speed	20 MHz
19.		Flash	32 k Byte
20.		Programmable I/O	23 Line

Sensors are used to measure throttle valve opening, braking, and steering speeds, through a Direct Current (DC) motor. The signal generated by these components is observed as a calibrated analog through a tachometer (mm/s). The calibration process was subsequently carried out by rotating the sensor with a DC motor, whose speed was adjusted by the controller. The signal generated was then processed by a conditioning circuit containing a rectifier and filter. Using NI data acquisition board, the signal conditioning outputs were displayed by the computer. These data were then compared with the tachometer reading values, as the sensor calibration scheme is shown in Fig. 2. (Calibration of DC motor as rotational speed sensor).

2.2. Research Equipment Set-up

The equipment installation set-up is shown in Fig. 3. The calibrated sensor was mounted on a single shaft to the throttle valve (2), the brake pedal top (3), and the steering system (4), which were connected through the timing belt. The signal generated by the sensor is transferred to the developed control system as speed data (mm/s), where the throttle valve mark is observed as throttle valve opening speed data. The braking and steering signals were also observed as the driver's speed data when releasing/stepping on the brake pedal and turning the wheel.

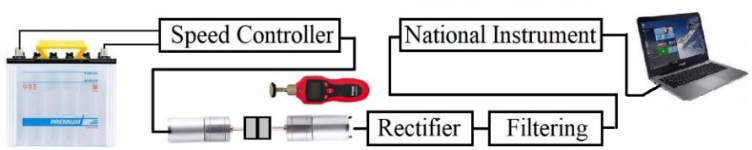

Fig. 2. Sensor calibration

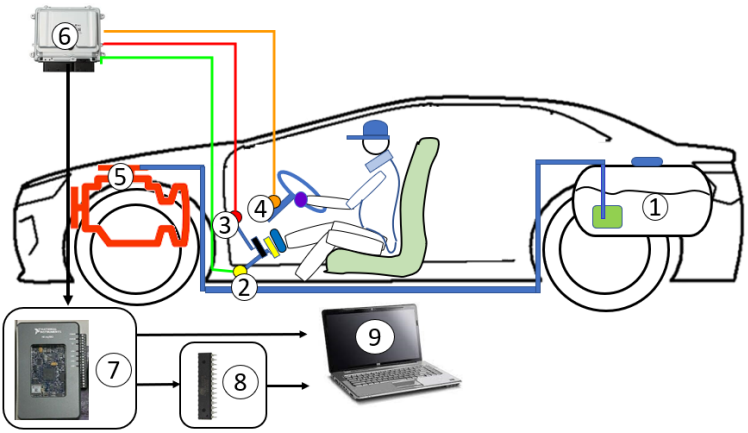

Description:
1. Fuel tank.
2. Throttle valve speed sensor.
3. Braking speed sensor.
4. Steering speed sensor.
5. Engine.
6. Developed control system.
7. Microcontroller NI MyRio.
8. IC ATmega 328.

Fig. 3. The equipment set-up

Furthermore, the developed control system (6) had two components, namely a NI MyRio microcontroller (7) and an IC ATmega 328 (8). The NI MyRio microcontroller helps to convert sensor speed data into acceleration parameters, with each information averaged within 15 mins. However, The IC ATmega 328 helps to process average acceleration change (mm/s^2) into a driver's behavior decision. This behavior was designed through a neural network trained and embedded in MATLAB Simulink and IC ATmega 328, respectively, with LEDs utilized as behavioral indicators. Besides the real-time identification of driver behavior, this study is expected to futuristically drive the fuel pump towards efficiently controlling the energy entering the engine (5). The changes are monitored through a computer (9) and an ATmega 328 IC-based LED.

2.3. Driving Behavior Recognition Control System Model

2.3.1. Acceleration Change Control System

The model of driving behavior control system used the acceleration change obtained from Eqs. (1). This calculation has an i value of 180 equations.

$$a_i = \frac{(v_i - v_{(i-1)})}{(t_i - t_{(i-1)})} \quad (1)$$

where: i = 1,2,…,180
a_i - Acceleration value at time i (mm/seconds^2),
t - Time of change of acceleration in units of seconds,
v_i - Speed value at time i (mm/seconds),
$v_{(i-1)}$ - Speed value at time i -1 (mm/seconds).

The acceleration control system is obtained from the change in speed at i (v_i) at the time i (t_i) minus the current speed at i -1(v_{i-1}) at time i-1 (t_{i-1}). The process of collecting speed data to be converted to acceleration is carried out every 5 seconds for 15 minutes (900 seconds), with data having a value of N 180 based on Eq. (1). These equations were created in the LabVIEW NI MyRio software, which was realistically connected to the sensors of the throttle-valve opening, braking, and in-vehicle steering speeds, respectively. Driving behavior is a set of attitudes when driving a vehicle for a long time. Driving behavior is designed to have two schemes, including eco, and stoichiometry schemes. The driving behavior scheme occurs because it has similarities between the driver's attitudes in a certain time and does not occur in a very short time (seconds), so data retrieval within 5 seconds is sufficient to describe the driver's behavior scheme. The driving behavior that falls into the eco scheme category is formed because of the similarity of smooth behavior that occurs at a certain time. So are the driving behavior stoichiometry schemes.

2.3.2. Calculation of Acceleration Change Average

Using the Moving Average (MA) formula, the changes in the average acceleration began from Eqs. (2).

$$MA_i = \frac{a_i + a_{i+1} + a_{i+2}}{3} \quad (2)$$

where: i = 1,2,…,180
MA_i - Average acceleration (mm/seconds^2).
a_i - Acceleration value at time i (mm/seconds^2).
a_{i+1} - Acceleration value at time i+1 (mm/seconds^2
a_{i+2} - Acceleration value at time i+2 (mm/seconds^2).

A total of 178 results were obtained and averaged ($\overline{MA}$), subsequently leading to Eq. (3). These were then transferred to the neural network embedded in the ATmega 328 IC.

$$\overline{MA} = \frac{MA_1 + MA_2 + \cdots MA_{178}}{178} \quad (3)$$

The change in average acceleration ($\overline{MA}$) was also used to calculate the signal generated by the throttle valve, steering, and braking sensors. In addition, Eqs. (2) and (3) were created in LabVIEW NI MyRio 2015. The calculation of the throttle valve sensor's average acceleration $\overline{MA}$ is used to identify the behavior of the throttle valve opening denoted by M_{tv}. The calculation of the average acceleration $\overline{MA}$ of the braking sensor is used to recognize the behavior of the braking operation, denoted by M_{st}, and the calculation of the average acceleration $\overline{MA}$ of the steering sensor is used to identify the behavior of the steer operation, denoted by M_{br}.

2.3.3. Neural Network Control System Design

The design of the driver behavior control system was carried out using a neural network, where the algorithm method used was the Levenberg Marquardt training type (*trainlm*). This training performance is designed based on Mean Squared Error (MSE), using 3 inputs, 1 hidden layer, 1 output layer, and 300 nodes. Also, the layer types used were *logsig*, *tansig*, and *purelin* model, as the neural network training utilized Epoch 20,000 with a success rate of 99.93%. This developed design is shown in Fig. 4, with the neural network being created and embedded in the MATLAB Simulink and IC ATmega 328, respectively.

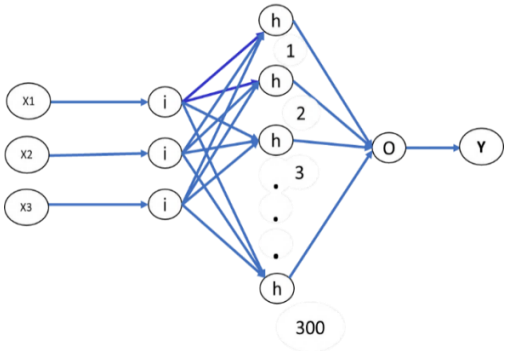

Fig. 4. The neural network design embedded in the ATmega 328 IC

2.4. Vehicle Engine Modeling Design

This prototype system is categorized into two models: vehicle engine modeling and driving behavior recognition design. Vehicle engine modeling was separately created in the MATLAB Simulink to describe the operation of the driving behavior control system. Meanwhile, the recognition control system modeling was created by the LabVIEW NI MyRio realistically installed on the vehicle. This modeling was used to identify the actual driving behavior. Data was also obtained in training the neural network to be included in the simulation vehicle engine modeling. In addition, the neural network was embedded in the IC ATmega 328 and used for fuel control in a future report. The designated modeling block diagram is shown in Fig. 5.

The vehicle engine modeling equation was in line with several previous studies (Setiyo M. & Munahar, 2017),(Sardarmehni et al., 2019). Based on this research, the vehicle engine modeling is divided into many parts, including the intake manifold pressure $\dot{P}_i$, the engine temperature $\dot{T}_i$, fuel dynamics $\dot{m}_{at}$, engine speed ($\dot{n}$), and vehicle dynamics.

The intake manifold pressure $\dot{p}_i$ is the dynamic modeling of the air entering the engine during operation due to the suction emanating from the piston movement, as shown in Eq. (4).

$$\dot{p}_i = \frac{k \cdot R}{V_i}\left(-\dot{m}_{ap} \cdot T_i + \dot{m}_{at} \cdot T_a + \dot{m}_{EGR} \cdot T_{EGR}\right) \quad (4)$$

The temperature of the air entering the engine $\dot{T}_i$ greatly affected the changes in combustion due to the process requiring a mixture of air and fuel. The temperature of the air entering the engine under actual conditions is measured by the IAT (Intake Air Temperature Sensor), as shown in Eq. (5).

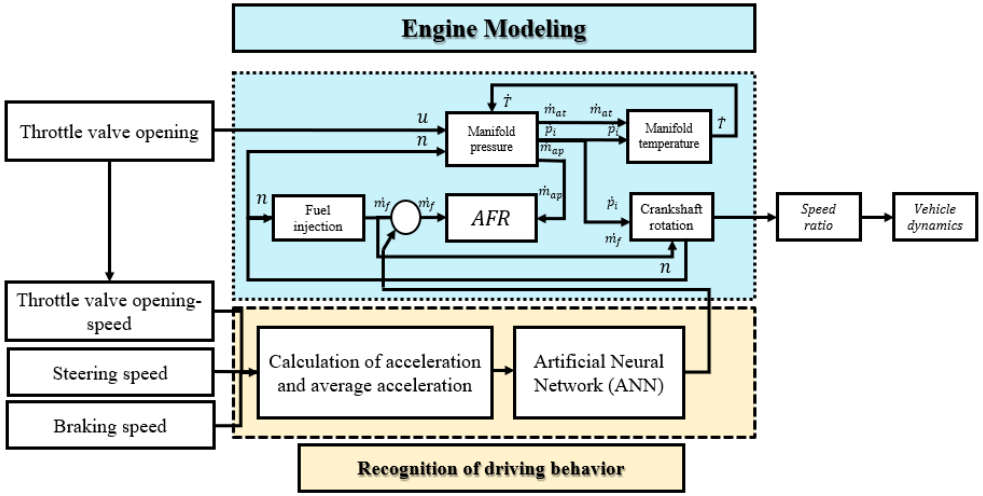

Fig. 5. The designated block diagram

$$\dot{T} = \frac{R \cdot T_i}{p_i \cdot V_i}\left[-\dot{m}_{ap}\,(k-1)T_i + \dot{m}_{at}\,(k \cdot T_a - T_i) + \dot{m}_{EGR}(k \cdot T_{EGR} - T_i)\right] \quad (5)$$

The dynamics of airflow in the throttle valve $\dot{m}_{at}$ also greatly affect the air pressure in the intake manifold $\dot{p}_i$ described in equations (6) and (7). $\beta_1(u)$ is the position of the throttle valve. $\beta_2 \cdot (p_r)$ is a function of p_r, which describes the ratio of manifold pressure to air pressure p_a. Air pressure entering the engine was measured using the Manifold Absolute Pressure Sensor (MAP). In this manifold, the air pressure was constantly changing $\dot{m}_{ap}$, depending on the engine speed ṅ and vehicle load. This sensor detected negative pressure in the chamber before entering the engine. The airflow in the throttle valve was also strongly influenced by position, as observed in Eqs. (8) and (10), where the m_{at0}, m_{at1}, u_0, and p_c are constant.

$$\dot{m}_{at}(u, p_i) = m_{at1} \cdot \frac{p_a}{\sqrt{T_a}}\beta_1(u) \cdot \beta_2 \cdot (p_r) + m_{at0} \quad (6)$$

$$\dot{m}_{ap}(n, p_i) = \frac{V_d}{120 \cdot R \cdot T_i}(\eta_i \cdot p_i)n \quad (7)$$

$$\beta_1(u) = 1 - \cos(u) - \frac{u_0^2}{2!} \quad (8)$$

$$p_r = \frac{p_i}{p_a} \quad (9)$$

$$\beta_2(p_r) = \sqrt{1 - \left(\frac{p_r - p_c}{1 - p_c}\right)} \text{ if } p_2 \geq p_c = 1 \text{ if } p_2 < p_c \quad (10)$$

Based on this study, the engine generated power to rotate the crankshaft (ṅ) used in driving the vehicle's load, as shown in Eq. (11) where P_p is the pumping power, η_i is efficiency, P_b is load and friction powers, P_f is friction power variables, $\dot{m}_f$ is the fuel flow entering the engine as shown in Eq. (12), ANN recognizes the driving behavior scheme to control $\dot{m}_f$, λ is a ratio between the stoichiometry and actual AFR value calculated in equation 13), $\Delta\tau_d$ is the injection delay time when the fuel was sprayed into the combustion chamber, and L_{th} is the stoichiometry AFR at 14.7 (Wu & Tafreshi, 2019).

$$\dot{n} = -\frac{1}{ln}\left(P_f(p_i, n) + P_p(p_i, n) + P_b(n)\right) + \frac{1}{ln}H_u.\eta_i(p_i, n, \lambda)\dot{m}_f(t - \Delta\tau_d) \quad (11)$$

$$\dot{m}_f = \frac{\dot{m}_{ap}}{L_{th}} \quad (12)$$

$$\lambda = \frac{\dot{m}_{ap}}{\dot{m}_f} \quad (13)$$

According to Eq. (14)-(18), $\dot{m}_{ff}$ is the mass of the fuel oil film, $\dot{m}_{f1}$ is the energy emanating from the injector, $\dot{m}_{fv}$ is the fuel flow entering the engine as a fog, n is the crankshaft rotation, τ_f is the fuel vaporization time constant and X_f is the energy deposited in the intake manifold chamber.

$$\dot{m}_{ff} = \frac{1}{\tau_f}(-m_{ff} + X_f \times \dot{m}_{f1}) \quad (14)$$

$$\dot{m}_{fv} = (1 - X_f)\dot{m}_{f1} \quad (15)$$

$$\dot{m}_f = \dot{m}_{fv} + \dot{m}_{ff} \quad (16)$$

$$X_f(\mathrm{p_i}, \mathrm{n}) = -0.277\mathrm{p_i} - 0.055\mathrm{n} + 0.68 \quad (17)$$

$$\begin{aligned}\tau_f(\mathrm{p_i}, \mathrm{n}) &= 1.35 \times (-0.672\mathrm{n} + 1.68) \\ &\times (\mathrm{p_i} - 0.825)(\mathrm{p_i} - 0.825)^2 \\ &+ (0.06 \times \mathrm{n} + 0.15) + 0.56\end{aligned} \quad (18)$$

The vehicular dynamics were strongly influenced by the moment of inertia I_v, which is the tendency to maintain its position due to the forces acting on the vehicle body. Vehicles have wheels to deliver loads at various rotational speeds N_w, as the engine rotation torque was changed for load movability with the transmission R_{TR}. It was also divided into the wheels with the final drive R_{fd}, as T_{load} was observed as the torque driving the load in Eq. (26). Based on Eqs. (19)-(25), T_{out} and T_{in} are the torques emanating from the transmission output and the clutch output/transmission input, respectively, N_{in} and N_{out} are the rotations entering and exiting the transmission input and output, respectively, R_{load0} and R_{load2}= the aerodynamic drag coefficients and friction, T_{brake} is a brake torque, and *mph* is vehicle's linear velocity, T_{in} is the transmission input torque (clutch output torque), K is the K-factor capacity, $\mathrm{N_e}$ = engine speed, f_1 is the ratio factor of the clutch's ability to transmit engine torque, f_2 is the ratio factor of the clutch disc's ability to transmit engine torque, RTQ is the engine torque ratio resulting from the clutch, f_3 is the gear speed ratio in the transmission.

$$T_{in} = \frac{{N_e}^2}{K^2} \times RTQ \quad (19)$$

$$K = f_1 \times \frac{N_{in}}{N_e} \quad (20)$$

$$RTQ = f_2 \times \frac{N_{in}}{N_e} \quad (21)$$

$$R_{TR} = f_3(gear) = Transmission\ ratio \quad (22)$$

$$I_v \times N_w = R_{fd}(T_{out} - T_{load}) \quad (23)$$

$$T_{out} = R_{TR} \times T_{in} \quad (24)$$

$$N_{in} = R_{TR} \times N_{out} \quad (25)$$

$$T_{load} = sgn(mph) \times (R_{load1} + R_{load2} mph^2 + T_{brake}) \quad (26)$$

2.5. Driving Behavior Recognition Cluster

Driving behavior was identified by throttle-valve opening, steering, and braking operations, through three schemes: the economizer (Eco), stoichiometry, and sporty. Eco and sporty schemes were calibrated based on previous studies. The results showed that the eco-scheme driver was determined when the behavior smoothly operated the vehicle through busy urban streets between 40-60 km/h (Vaezipour, Rakotonirainy, & Haworth, 2018). The sporty-scheme driver was determined when the behavior quickly operated the vehicle through a high and adventurous spirit above 80 km/h (Reinolsmann et al., 2019). Meanwhile, the stoichiometry scheme was determined based on the range between eco and sporty behaviors, as shown in Table 2. Therefore, this study only focused on the applications of driving behavior to the eco and stoichiometry schemes.

Table 2. Driving Behavior Schemes

No.	Scheme of driving behavior	Type of driving operation		
		M_{tv}	M_{st}	M_{br}
1.	A	1	1	1
2.	B	1	1	2
3.	B	1	2	1
4.	B	1	1	3
5.	B	1	2	2
6.	B	2	2	2
7.	B	2	1	1
8.	B	2	2	1
9.	B	2	1	2
10.	B	1	2	3
11.	B	1	3	2
12.	B	1	3	3
13.	B	1	3	1
23.	B	2	2	3
24.	B	2	3	3
25.	B	2	3	2
26.	B	2	3	1
27.	B	2	1	3

Note : A = Economizer, B= Stoichiometry, Low = 1, Medium = 2, and High = 3.

3. Result and Discussion

The driving behavior was designed with three inputs: throttle-valve opening acceleration, braking, and steering operations. The operating behavior of the throttle valve opening acceleration is obtained from the sensor signal mounted at the end of the TPS (Throttle valve Position Sensor) shaft. The result was subsequently used as the throttle valve opening speed data when the driver increased/decreased the vehicle velocity. The data collection of this behavior was also carried out for 2,700 seconds (45 minutes), with the control system being designed to provide periodic decisions every 15 minutes (900 seconds). Additionally, the throttle valve opening speed signal is shown in Fig. 6.

3.1. Throttle Valve Operation Behavior

The driving behavior for the throttle valve opening operation has different behavior, which is presented in Figure 6. In the first period (0-900 s), the throttle valve opening behavior has a speed of 0 - 3.5 mm/s. In the second period (901-1800 s), the throttle valve opening behavior was 0.5 - 3.8 mm/s. The third period (1801- 2700 s) was in the range of 0.5 - 3.4 mm/s.

The throttle-valve opening speed data, generated using Eqs. (1)-(3) and the sensor at the end of the TPS was then converted into acceleration parameters, as shown in Fig. 7. in which the average value of throttle-valve opening acceleration M_{tv} had a value of 0.001 mm/s^2 (low range) in the first and second 900 seconds. Meanwhile, an average value of 0.002 mm/s^2 (medium-range) was observed in the third period. At 2,700 seconds (45 minutes), two different throttle-valve opening behaviors were produced, namely low and medium scales. The clustering of the average throttle-valve opening acceleration values refers to Table 3.

3.2. Steering Operation Behavior

Steering operation is the driver's behavior when turning the vehicle wheels left or right. This operation was measured by attaching sensors to the steering wheel connected to a timing belt, and this sensor produced an analog signal, which provided steering speed data. The data collection period was also carried out for 2,700 seconds (45 minutes) when the vehicle was operating under different conditions. For the first, second, and third 900 s, the steering operation had speeds of 0-170, 0-160, and 0-200 mm/s, respectively. The value of the change in steering operating speed is presented in Fig. 8.

Using Eqs. (1)-(3), these results were then converted into steering acceleration data, which were subsequently inputted into the LabVIEW NI MyRIO software. The changes in the processed steering acceleration M_{st} are shown in Fig. 9, as the procedure was carried out for 15 minutes (900 seconds), with data retrieved every 5 seconds

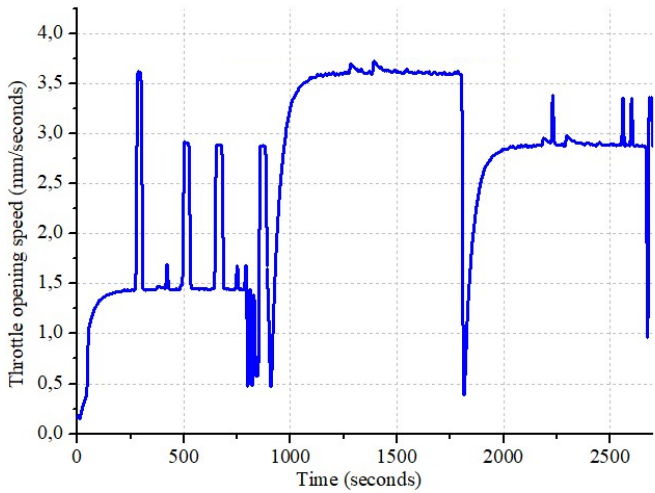

Fig. 6. The signal of throttle valve opening speed

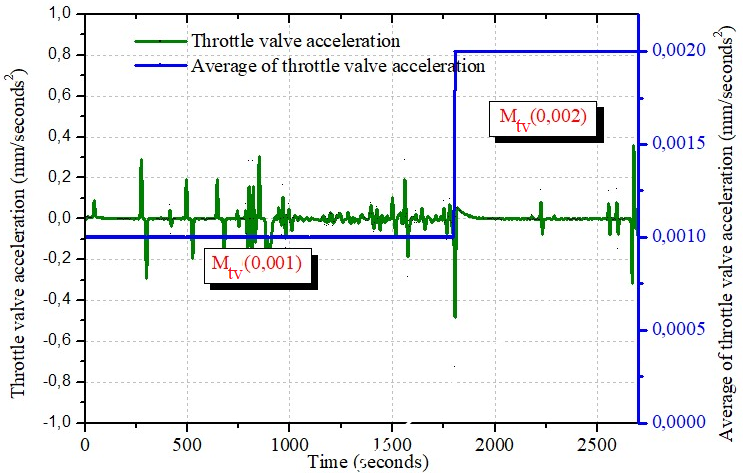

Fig. 7. Changes in throttle opening acceleration behavior

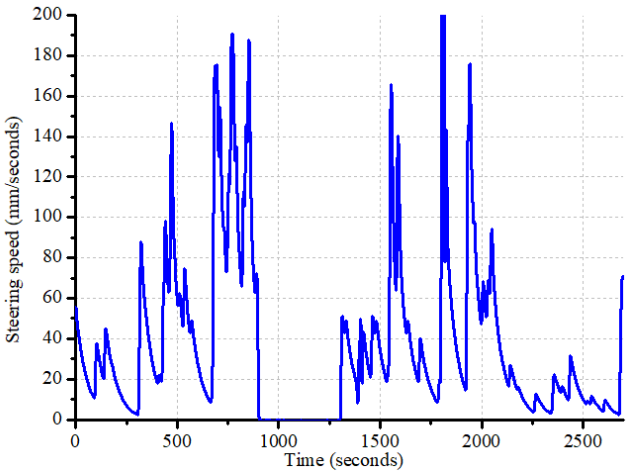

Fig. 8. Steering operating speed signal

The data collection process was carried out as many as 180 data, with a range of retrieval of 2,700 seconds (45 minutes).In the first, second, and third 900 seconds, the average values of steering acceleration were 0.00 (low range), 0.019 (low range), and 0.05 mm/s^2 (medium range), respectively. These average values that two different steering operating behaviors were produced for 2,700 seconds (45 minutes), namely the low and high scale accelerations. The clustering of the average steering acceleration values refers to table 3.

3.3. Braking Operation Behavior

Braking operation is the behavior observed when the driver steps on the brake pedal to reduce or stop the vehicle movement. This behavior was measured by attaching a sensor to the brake pedal's end, producing an analog signal with braking speed data. The data collection period was also carried out for 2,700 seconds, with the vehicle operating under different conditions. In the first, second, and third 900 seconds, the braking operation had speed values of 0.5-(-1), (-1)-1, and 0-2.7 mm/s. The value of the change in steering operating speed is shown in Fig. 10.

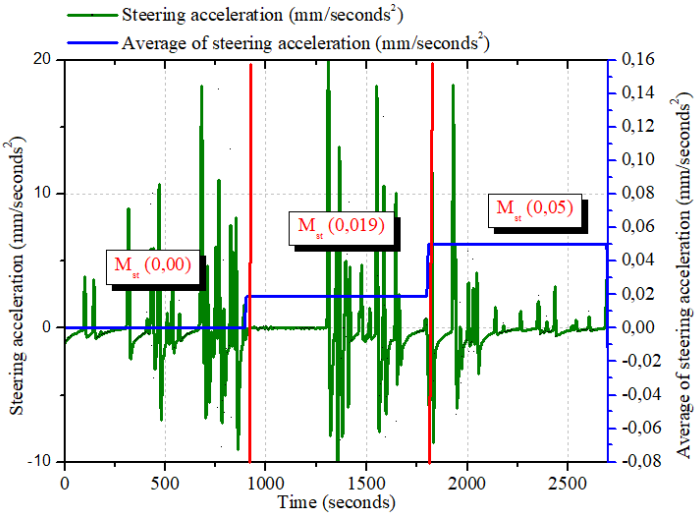

Fig. 9. Changes in steering operation acceleration behavior

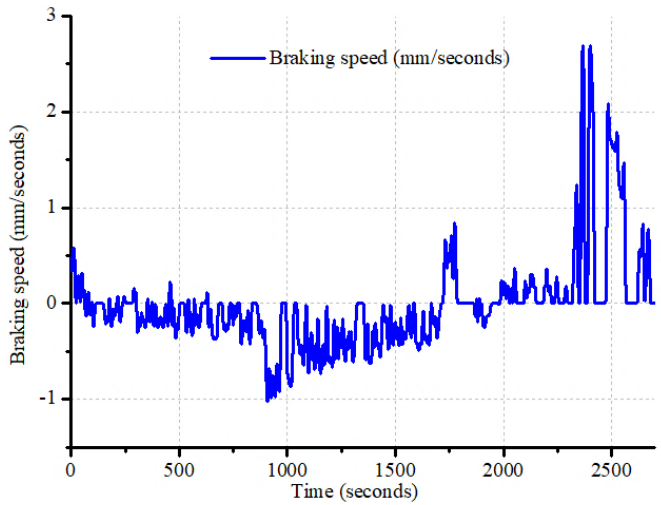

Fig. 10. Braking operation speed signal

Using Eqs. (1)-(3), the sensor-based braking operating speed data were then converted into acceleration parameters, with the results being presented in Fig. 11. This process was carried out for 15 minutes (900 seconds), with data being retrieved every 5 seconds. A total of 180 data were also obtained during this process, with the range of retrieval conducted for 2700 s (45 minutes). The results showed that the average braking acceleration M_{br} had speed values of -0.0004 (medium range), 0.0001 (low range), and 0.0002 mm/s^2 (low range) for the first, second, and third 900 s, respectively. At 2700 s (45 minutes), three different operating behaviors were produced: the medium, high, and low scales. The clustering of the average braking acceleration values refers to table 3. The calibration of the cluster average of throttle valve operation M_{ts} steering M_{st}, and braking accelerations M_{br} are presented in Table 3, where the range is based on the driving scheme behavior as a fuel controller.

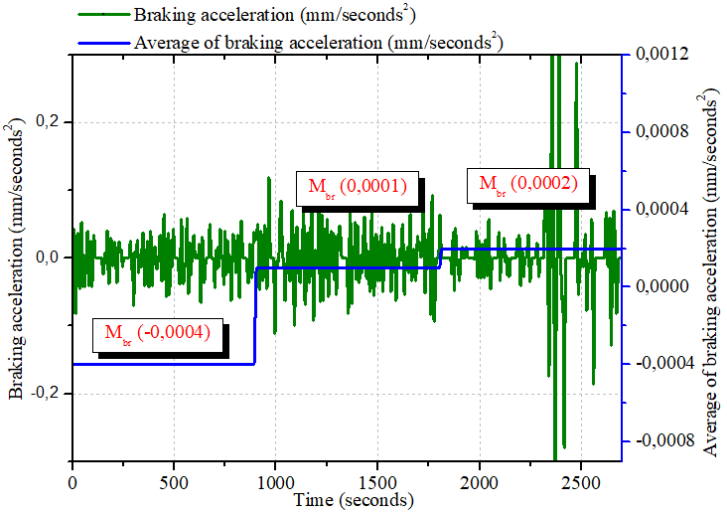

Fig. 11. Changes in braking operation acceleration behavior

Table 3. The cluster average range of throttle valve operation $\boldsymbol{M_{ts}}$, steering $\boldsymbol{M_{st}}$ and braking acceleration $\boldsymbol{M_{br}}$

Description	Low (mm/seconds²)	Medium (mm/seconds²)	High (mm/seconds²)
M_{tv}	(-0.001)-0.001	0.002	0.003
M_{st}	(-0,02) – 0.02	(-0.05) – (-0.03) & 0.03 – 0.05	(-0.08) – (-0.06) & 0.06 – 0.08
M_{br}	(-0.0003)-0.0003	(-0.0009) – (-0.0006) & 0.0006 –0.0009	(-0.005) – (-0.001) & 0.001 – 0.005

3.4. Vehicle Engine Modeling Results

The MATLAB Simulink engine model also simulated the calculations of the driving behavior control system when operating a vehicle. The simulation began by placing the throttle-valve position at 24-36% for 2,700 seconds, indicating the level of the sensor component when periodically opened from an angle of 24-36%, as shown in Fig. 12.

The throttle-valve opening position also operated the engine towards the rotation of the crankshaft, whose motion was based on the power generated. In this process, the engine was rotated from 3,000-4,000 rpm in 0-2,700 seconds, as shown in Fig. 13.

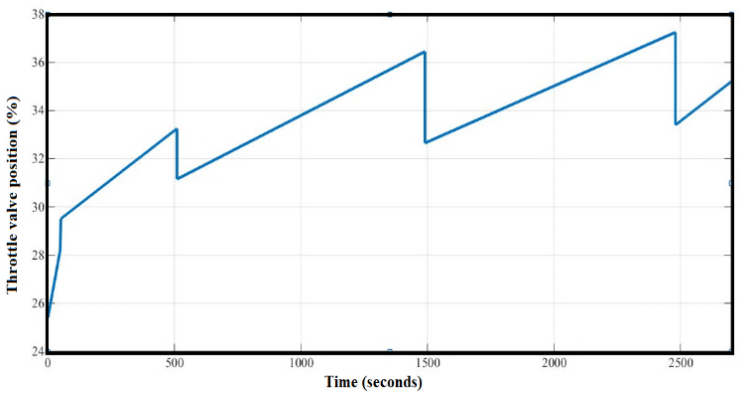

Fig. 12. Simulation of throttle valve opening position

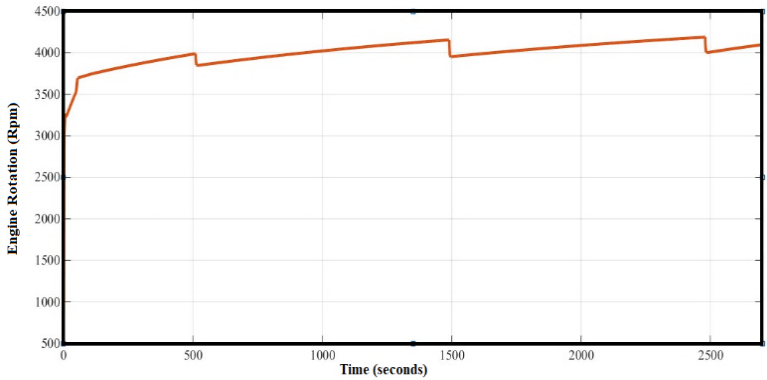

Fig. 13. Engine speed simulation

After the engine ignition, the vehicle was operated on a simulated scale between 0-160 km/h. This process vehicle speeds depending on the engine velocity and throttle-valve opening position. The process was also carried out using the transmission in the speed gear position 5. Additionally, the variational vehicle speed and transmission modeling are presented in Figs. 14 and 15, respectively.

The neural network control system was then included in the vehicle engine modeling based on actual driver behavior. The occurrences within the first and third 900 seconds were observed in the stoichiometry scheme, with the second period in the eco group, as presented in Fig. 16.

According to the driving behavior control system, the obtained identifications were used to control fuel flow entering the engine. This fuel-saving process increased with the entrance of driving behavior into the eco scheme through smooth driving processes on steering, braking, and throttle-valve opening levels. The vehicle also traveled between 40-60 km/h, operating on a busy urban road. In this process, the driving behavior control system reduces the fuel entering the engine, increasing energy-saving. The condition was also crucial due to fewer power requirements in the eco scheme. Based on the driving behavior control system, the fuel flow/AFR differences had a very significant range of values, with the increased fuel-saving processes observed in at 900 - 1,800 s (second period). Using this system, the AFR also had a value above 14.7, with achievement at 16. The fuel-saving value was adequately achieved with optimal engine power in this condition. The fuel flow also had a lower rate at 900 -1800 seconds, as presented in Figs. 17 and 18.

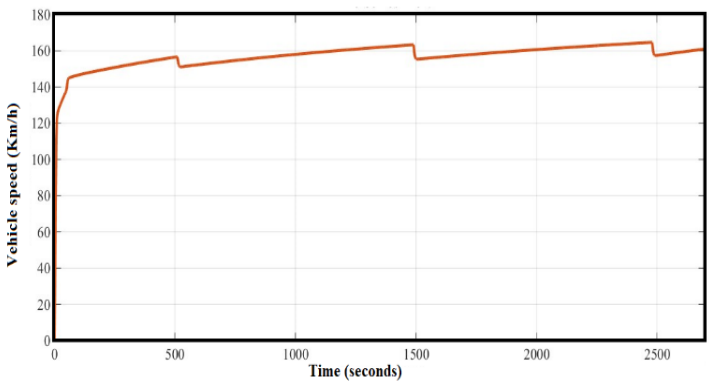

Fig. 14. Simulation of vehicle speed variations

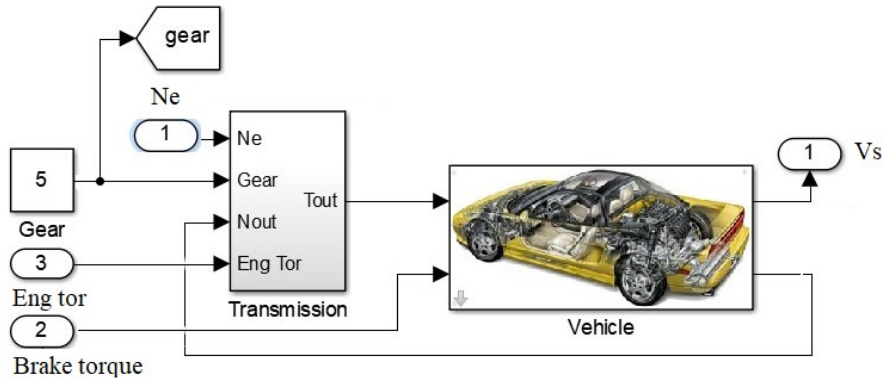

Fig. 15. Transmission modeling in vehicles

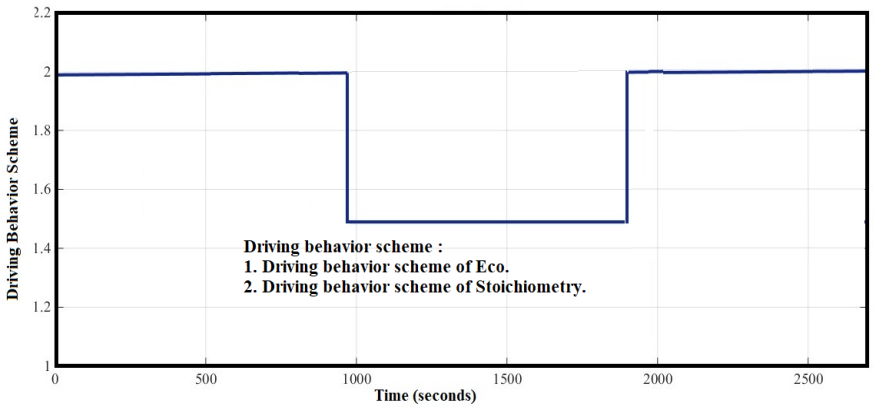

Fig. 16. Driver behavior recognition results based on neural networks

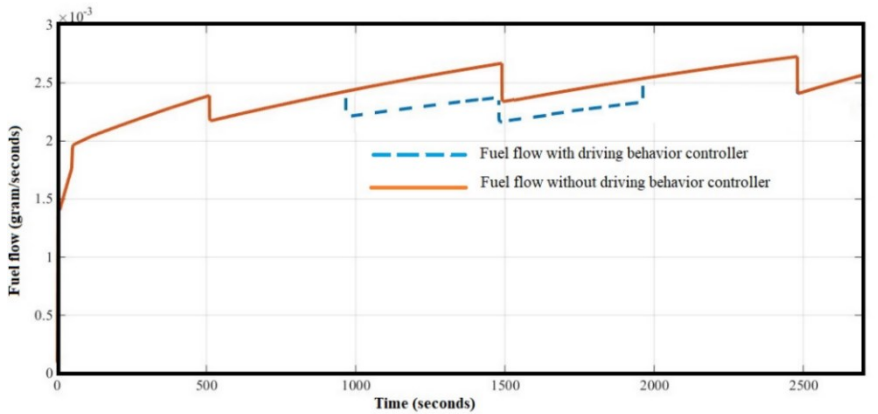

Fig. 17. Differences in fuel flow between control systems with and without driving behavior

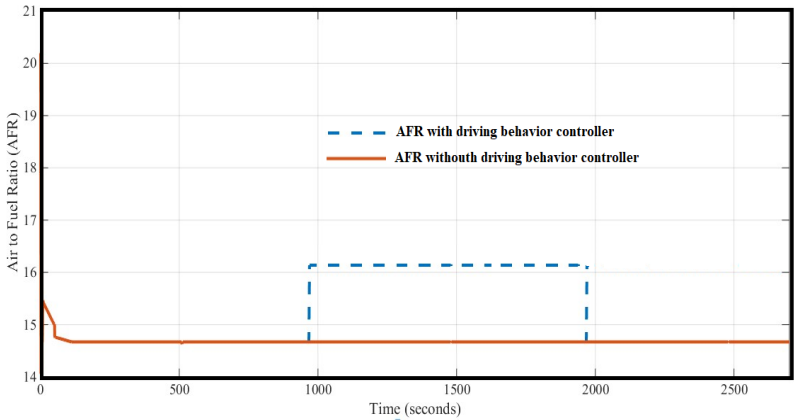

Fig. 18. AFR differences between control systems with and without driving behavior

The developed control system also provided an advantage over several previous studies due to the increase of the fuel AFR above the stoichiometry value (14.7) when the driver did not need much power. This advantage was observed from the smooth driver behavior when driving a vehicle. Based on the Fuel Saving Index (FSI) assessment analysis, the vehicle AFR, at 900 - 1,800 seconds, entered the cluster IV area. This area has a good savings rate and produces optimal engine power, which suits driver behavior in eco conditions. The results of the FSI analysis in this study are presented in Fig. 19. Research that has been done proves that the fuel economy achieved is better than in previous studies, which only led to stoichiometric AFR (Ahmed & Al, 2019)(Sardarmehni et al., 2019). The AFR achieved is in the AFR 16 range (above stoichiometry) when the steering behavior is in an eco scheme.

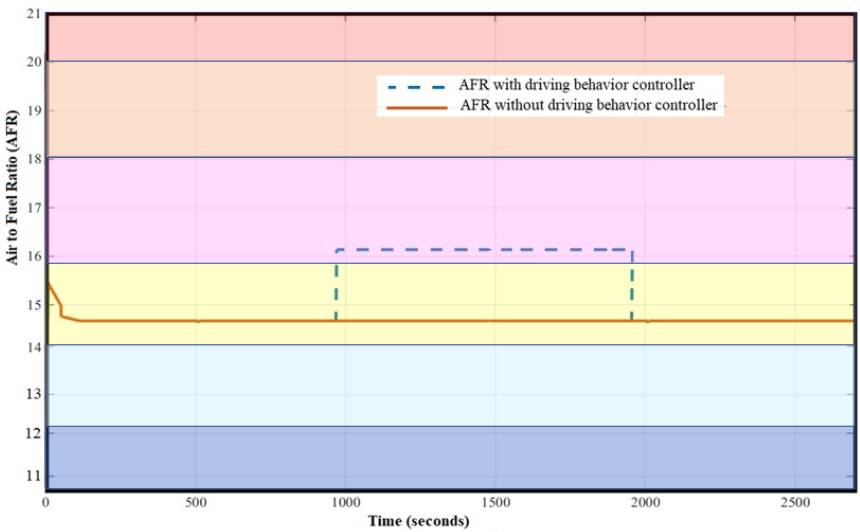

Fig. 19. The results of the FSI assessment analysis for achieving AFR on the control system with driver behavior using a neural network

FSI as an AFR assessment has several conditions, presented in table 4. FSI Class I has a pink color with an AFR value above 20. This cluster produces the highest fuel economy. However, the power generated is very poor, and the engine barely operates. FSI class II is brown with an AFR value of 18 – 20. The fuel economy effect is very good. However, the power generated is not good. The machine can only operate with light loads. FSI class III is purple with an AFR value of 16 - 18. Good fuel economy effect. The power generated is quite good. The machine can operate with a heavier load. FSI class IV is yellow with an AFR value of 14 – 16. The fuel-saving effect is quite good. The engine produces the most optimal power with a range of 70-80%. FSI class V with a light blue color code with an AFR value of 12 – 13. This class has relatively poor fuel economy. Maximum power generated. FSI class VI with dark blue color code with AFR values 11 – 12. The resulting fuel economy is very bad. This class produces engine power that begins to fall.

Table 4. FSI cluster for AFR assessment

I	IV
II	V
III	VI

The research that has been carried out is in line with the suggestions from previous researchers, which stated that driver behavior has a close relationship with fuel consumption (Xing et al., 2020). In addition, the analysis of the FSI assessment to achieve AFR on the designed control system refers to the previous reference (Martyr & Plint, 2007).

4. Conclusion

Using a neural network, the driving behavior control system designed in a LabVIEW NI MyRio has been successfully embedded in the ATmega 328 IC. This modeling realistically identified the driving behavior during vehicle operations. The results of the introduction of driver behavior using a neural network in the first period (0-900 s) and third (1801 - the 2700s) entered the stoichiometry scheme, while the second period (901 - 1800 s) entered the eco scheme. The throttle valve operating behavior in the first and second periods is in a low range (0.001), while the third period is in the medium range (0.002). The steering operations behavior in the first and second periods is in a low range (0.00 and 0.019), while the third period is in the medium range (0.05). The braking operation behavior in the second and third periods is in a low range (0.0001 and 0.0002), while the first period is in the medium range (-0.0004). Meanwhile, the MATLAB Simulink engine modeling successfully simulated the performance of the driving behavior control system when operating in a vehicle to increase fuel-saving. The fuel-saving achieved was also included in the cluster IV FSI due to having the best index and the most optimal engine power. The AFR achieved is in the AFR 16 range (above stoichiometry) when the steering behavior is in an eco scheme. Subsequently, this FSI had six clusters, namely Cluster I had poor FSI due to the inability of the engine to operate (AFR above 20). Cluster II had excellent FSI and lacked engine power. Cluster III had very good FSI and a quite optimal engine power. Cluster IV had good FSI and optimal power. Cluster V had poor FSI and maximum engine power, and Cluster VI had poor FSI and engine power. Based on this study, the design of a prototype neural network-based driving behavior control system was successfully operated on a simulation scale, where the results obtained had a very high success rate. This concept can be used in EVs, FCs, alternative fuel vehicles, and hydrogen. However, the system did not consider the aspect of safety, which should be an essential development priority for subsequent future studies.

Acknowledgment

Thank you to the Robotics Laboratory of Mechanical Engineering and the Electrical Engineering Laboratory of Diponegoro University for their support. In addition, thanks are also conveyed to the automotive engineering laboratory and LPPM Muhammadiyah Magelang University, who have funded this research.

Nomenclature

I_v	Moment of inertia
k	Heat specification ratio (1.4)
K	K-factor capacity
L_{th}	AFR stoichiometry (14.7)
$\dot{m}_f$	The dynamics of gasoline entering the combustion chamber (kg/s)
m_{ff}	Mass of fuel film (kg/s)

$\dot{m}_{fv}$ Gasoline flow in the form of steam (kg/s)
$\dot{m}_{ap}$ Mass flow of air to the engine (kg/s)
$\dot{m}_{at}$ Airflow at throttle valve (kg/s)
$\dot{m}_{EGR}$ Exhaust airflow (kg/s)
M_{tv} Average $\overline{MA}$ of throttle valve opening acceleration
M_{st} Average $\overline{MA}$ of braking acceleration
M_{br} Average $\overline{MA}$ of steering acceleration
N_{in} The speed at transmission input (rpm)
N_{out} The speed at transmission output (rpm)
N_e Engine speed (rpm)
N_w Wheel speed (rpm)
N_{in} Transmission input rotation (rpm)
$\dot{\boldsymbol{n}}$ Crankshaft rotation (krpm)
ηi Efficiency indication
N_e Engine speed (rpm)
$\dot{P}_i$ Intake manifold pressure (bar)
P_b Load power (kW)
P_f Friction power (kW)
P_p Pumping power (kW)
R Gas constant (287×10^{-5}).
R_{fd} Final drive ratio
R_{load0} Friction drag coefficient
R_{load2} Aerodynamic drag coefficient
RTQ Engine torque ratio
R_{TR} The speed gear ratio on transmission
T_a Ambient temperature (kelvin)
$\dot{T}_i$ Air temperature (kelvin).
T_{load} Load torque
T_{out} Transmission output torque
T_{brake} Braking torque
T_{in} Torque on the transmission input shaft (kg.m)
T_{EGR} Exhaust gas temperature (kelvin)
u Throttle position (%)
V_i Intake manifold volume (m^3)
X_f Fuel deposited in the inlet to the engine (kg/s)
$\boldsymbol{\lambda}$ Lambda
$\Delta\tau_d$ Injection time delay (seconds)
τ_f Fuel evaporation time constant

References

[1] Ahmed, S., & Al, F. (2019). Analyzing and predicting the relation between air – fuel ratio (AFR), lambda (λ) and the exhaust emissions percentages and values of gasoline - fueled vehicles using versatile and portable emissions measurement system tool. *SN Applied Sciences*, *1*(11), 1-12. DOI: 10.1007-/s42452-019-1392–1395.

[2] Al-fattah, S. M. (2020). Non-OPEC conventional oil : Production decline , supply outlook and key implications. *Journal of Petroleum Science and Engineering*, *189*, 107049. DOI: 10.1016/j.petrol.-2020.107049.

[3] Alper, A., & Do, Y. (2018). Investigation of the effects of gasoline and CNG fuels on a dual sequential ignition engine at low and high load conditions. *Fuel*, *232*(May), 114-123. DOI: 10.1016/j.fuel.-2018.05.156.

[4] Ashkrof, P., Homem, G., Correia, D. A., & Arem, B. Van. (2020). Analysis of the effect of charging needs on battery electric vehicle drivers ' route choice behaviour : A case study in the Netherlands. *Transportation Research Part D*, *78*, 102206. DOI: 10.1016/j.trd.2019.102206.

[5] Biswal, A., Gedam, S., Balusamy, S., & Kolhe, P. (2020). Effects of using ternary gasoline-ethanol-LPO blend on PFI engine performance and emissions. *Fuel*, *281*(July), 118664. DOI: 10.1016/j.fuel.-2020.118664.

[6] Fadhloun, K., & Rakha, H. (2020). A novel vehicle dynamics and human behavior car-following model : Model development and preliminary testing. *International Journal of Transportation Science and Technology*, *9*, 14-28. DOI: 10.1016/j.ijtst.2019.05.004.

[7] Grove, K., Soccolich, S., Engström, J., & Hanowski, R. (2019). Driver visual behavior while using adaptive cruise control on commercial motor vehicles q. *Transportation Research Part F: Psychology and Behaviour*, *60*, 343-352. DOI: 10.1016/j.trf.2018.10.013.

[8] Hong, Z., Chen, Y., & Wu, Y. (2020). A driver behavior assessment and recommendation system for connected vehicles to produce safer driving environments through a " follow the leader " approach. *Accident Analysis and Prevention*, *139*(November 2019), 105460. DOI: 10.1016/j.aap.2020.105460.

[9] Kohl, J., Gross, A., Henning, M., & Baumgarten, T. (2020). Driver glance behavior towards displayed images on in-vehicle information systems under real driving conditions. *Transportation Research Part F: Psychology and Behaviour*, *70*, 163-174. DOI: 10.1016/j.trf.2020.01.017.

[10] Martinelli, F., Mercaldo, F., Orlando, A., Nardone, V., Santone, A., & Kumar, A. (2020). Human behavior characterization for driving style recognition in vehicle system R. *Computers and Electrical Engineering*, *83*, 102504. DOI: 10.1016/j.compeleceng.2017.12.050.

[11] Martyr, A. ., & Plint, M. . (2007). *Engine Testing Theory and Practice*. Elsevier Ltd. Retrieved from https://id1lib.org/book/563256/1abf18

[12] Mehra, R. K., Duan, H., Luo, S., Rao, A., & Ma, F. (2018). Experimental and arti fi cial neural network (ANN) study of hydrogen enriched compressed natural gas (HCNG) engine under various ignition timings and excess air ratios. *Applied Energy*, *228*(April), 736-754. DOI: 10.1016/j.apenergy.-2018.06.085.

[13] Monika, A. Z., Chlopek, Z., Merkisz, J., & Pielecha, J. (2022). Analysis of The Operation State of Internal Combustion Engine in The Real Driving Emissions Test. *Archives of Transport*, *61*(1), 71–88. DOI: 10.5604/01.3001.0015.8162.

[14] Munahar, S., Condro, B., Muji, P., Aris, S., Joga, T., & Setiawan, D. (2020). Design and application of air to fuel ratio controller for LPG fueled vehicles at typical down - way. *Springer Nature*, (August 2019), https://doi.org/10.1007/s42452-019-1839-8. DOI: 10.1007/s42452-019-1839-8.

[15] Nguyen, K., & Nguyen, V. (2018). Energy for Sustainable Development Study on performance enhancement and emission reduction of used fuel-injected motorcycles using bi-fuel gasoline-LPG. *Energy for Sustainable Development*, *43*, 60-67. DOI: 10.1016/j.esd.2017.12.005.

[16] Reinolsmann, N., Alhajyaseen, W., Brijs, T., Pirdavani, A., Hussain, Q., & Brijs, K. (2019). Investigating the impact of dynamic merge control strategies on driving behavior on rural and urban expressways – A driving simulator study. *Transportation Research Part F: Traffic Psychology and Behaviour*, *65*, 469-484. DOI: 10.1016/j.trf.2019.08.010.

[17] Robertson, D., & Prucka, R. (2020). Evaluation of autoignition models for production control of a spark-assisted compression ignition engine. *International Journal of Engine Research*, 1-13. DOI: 10.1177-/1468087420934555

[18] Sardarmehni, T., Aghili Ashtiani, A., & Menhaj, M. B. (2019). Fuzzy model predictive control of normalized air-to-fuel ratio in internal combustion engines. *Soft Computing*, *23*(15), 6169-6182. DOI: 10.1007/s00500-018-3270-2.

[19] Setiyo M. & Munahar, S. (2017). AFR and fuel cut-off modeling of LPG-fueled engine based on engine , transmission , and brake system using fuzzy logic controller (FLC). *Journal of Mechatronics, Electrical Power, and Vehicular Technology*, *8*, 50-59. DOI: 10.14203/j.mev.2017.v8.50-59.

[20] Sharma, A., Zheng, Z., Bhaskar, A., & Haque, M. (2019). Modelling car-following behaviour of connected vehicles with a focus on driver compliance. *Transportation Research Part B*, *126*, 256-279. DOI: 10.1016/j.trb.2019.06.008.

[21] Stogios, C., Kasraian, D., Roorda, M. J., & Hatzopoulou, M. (2019). Simulating impacts of automated driving behavior and traffic conditions on vehicle emissions. *Transportation Research Part D*, *76*, 176-192. DOI: 10.1016/j.trd.2019.09.020.

[22] Sun, B., Zhang, T., GE, W., Tan, C., & Gao, S. (2019). Driving Energy Management of Front - AND - Rear - Motor - Drive Electric Vehicle Based on Hybrid Radial Basis Function. *Archives of Transport*, *49*(1), 47–58. DOI: 10.5604/01.3001.0013.2775.

[23] Uslu, S., & Celik, M. B. (2020). Performance and Exhaust Emission Prediction of a SI Engine Fueled with I amyl Alcohol-Gasoline Blends : An ANN Coupled RSM Based Optimization. *Fuel*, *265*, 116922. DOI: 10.1016/j.fuel.2019.116922

[24] Vaezipour, A., Rakotonirainy, A., & Haworth, N. (2018). A simulator evaluation of in-vehicle human machine interfaces for eco-safe driving. *Transportation Research Part A*, *118*, 696-713. DOI: 10.1016/j.tra.2018.10.022.

[25] Wang, P., Gao, S., Cheng, L., & Zhao, H. (2020). Research On Driving Behavior Decision Making System Of Autonomous Driving Vehicle Based On Benefit Evaluation Model. *Archives of Transport*, *53*(1), 21–36. DOI: 10.5604/01.3001.0014.1740.

[26] Wang, Y., Shi, Y., Cai, M., & Xu, W. (2020). Predictive control of air-fuel ratio in aircraft engine on fuel-powered unmanned aerial vehicle using fuzzy-RBF neural network. *Journal of the Franklin Institute*, *357*, 8342-8363. DOI: 10.1016/j.jfranklin.2020.03.016.

[27] Wu, H., & Tafreshi, R. (2019). Observer-based internal model air – fuel ratio control of lean-burn SI engines. *IFAC Journal of Systems and Control*, *9*, 100065. DOI: 10.1016/j.ifacsc.2019.100065.

[28] Xing, Y., Lv, C., Cao, D., & Lu, C. (2020). Energy oriented driving behavior analysis and personalized prediction of vehicle states with joint time series modeling. *Applied Energy*, *261*, 114471. DOI: 10.1016/j.apenergy.2019.114471.

[29] Xiong, H., Liu, H., Zhang, R., & Yu, L. (2019). An energy matching method for battery electric vehicle and hydrogen fuel cell vehicle based on source energy consumption rate. *International Journal of Hydrogen Energy*, *44*(56), 29733-29742. DOI: 10.1016/j.ijhydene.2019.02.169.

[30] Yuan, Y., Lu, Y., & Wang, Q. (2020). Adaptive forward vehicle collision warning based on driving behavior. *Neurocomputing*, *408*, 64-71. DOI: 10.1016/j.neucom.2019.11.024.

[31] Zhao, X., Wang, Z., Xu, Z., Wang, Y., Li, X., & Qu, X. (2020). Field experiments on longitudinal characteristics of human driver behavior following an autonomous vehicle. *Transportation Research Part C*, *114*, 205-224. DOI : 10.1016/j.trc.2020.02.018.